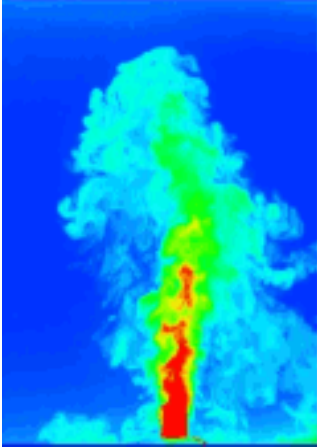


This article was downloaded by:[University Of Melbourne]  
On: 19 September 2007  
Access Details: [subscription number 773216479]  
Publisher: Taylor & Francis  
Informa Ltd Registered in England and Wales Registered Number: 1072954  
Registered office: Mortimer House, 37-41 Mortimer Street, London W1T 3JH, UK



## Journal of Turbulence

Publication details, including instructions for authors and subscription information:  
<http://www.informaworld.com/smpp/title~content=t713665472>

### Investigation of three dimensionality in the near field of a round jet using stereo PIV

B. Ganapathisubramani<sup>a</sup>; E. K. Longmire<sup>a</sup>; I. Marusic<sup>a</sup>

<sup>a</sup> Department of Aerospace Engineering and Mechanics, University of Minnesota, Minneapolis, MN, USA

First Published on: 21 March 2002

To cite this Article: Ganapathisubramani, B., Longmire, E. K. and Marusic, I. (2002) 'Investigation of three dimensionality in the near field of a round jet using stereo PIV', Journal of Turbulence, 3:1, 1 - 12

To link to this article: DOI: 10.1088/1468-5248/3/1/016

URL: <http://dx.doi.org/10.1088/1468-5248/3/1/016>

PLEASE SCROLL DOWN FOR ARTICLE

Full terms and conditions of use: <http://www.informaworld.com/terms-and-conditions-of-access.pdf>

This article maybe used for research, teaching and private study purposes. Any substantial or systematic reproduction, re-distribution, re-selling, loan or sub-licensing, systematic supply or distribution in any form to anyone is expressly forbidden.

The publisher does not give any warranty express or implied or make any representation that the contents will be complete or accurate or up to date. The accuracy of any instructions, formulae and drug doses should be independently verified with primary sources. The publisher shall not be liable for any loss, actions, claims, proceedings, demand or costs or damages whatsoever or howsoever caused arising directly or indirectly in connection with or arising out of the use of this material.

# Investigation of three dimensionality in the near field of a round jet using stereo PIV†

B Ganapathisubramani‡, E K Longmire and I Marusic

Department of Aerospace Engineering and Mechanics, University of Minnesota,  
107 Akerman Hall, 110 Union Street SE, Minneapolis, MN 55455, USA

E-mail: [bugs@aem.umn.edu](mailto:bugs@aem.umn.edu)

Received 9 October 2001

Published 21 March 2002

**Abstract.** A round air jet at a Reynolds number of 19 000 was studied using stereo PIV techniques in an effort to understand the characteristics of all three velocity components in the developing shear layer and to study the evolution of three dimensionality with increasing axial distance. Pulsed laser sheets were aligned to illuminate the centreline plane of the jet. The stereo PIV set-up was suitably calibrated to translate the resulting pixel displacements into axial, radial, and azimuthal velocity components. Details of measurement accuracy are discussed and related to the presence of local velocity gradients. Experimental results show that the RMS of the azimuthal velocity is of the order of  $0.1V_0$  in the shear layer downstream of  $y/D \sim 0.5$ . This is significantly earlier than reported in previous studies. Various feature extraction schemes based on the velocity gradient tensor were developed to identify the presence of the vortex cores and straining braid regions. Individual fields show that both vortex cores and braids are three dimensional. The braids contain streamwise vortex tubes while the cores can possess significant azimuthal velocity. The initial azimuthal perturbations typically were associated with straining regions immediately upstream of the first vortex ring that formed at the downstream location of  $y/D \sim 0.5$ .

PACS number: 47.27.Wg

† This article was chosen from Selected Proceedings of the Second International Symposium on Turbulence and Shear Flow Phenomena (KTH-Stockholm, 27–29 June 2001) ed E Lindborg, A Johansson, J Eaton, J Humphrey, N Kasagi, M Leschziner and M Sommerfeld.

‡ Author to whom any correspondence should be addressed.

---

## Contents

<b>1</b>	<b>Introduction</b>	<b>2</b>
<b>2</b>	<b>Experimental facility</b>	<b>2</b>
<b>3</b>	<b>Stereo PIV method</b>	<b>4</b>
3.1	Calibration . . . . .	4
3.2	Sources of uncertainty . . . . .	5
<b>4</b>	<b>Results and discussion</b>	<b>6</b>
4.1	Mean and RMS statistics . . . . .	6
4.2	Vortex identification . . . . .	7
4.3	Three dimensionality . . . . .	8
<b>5</b>	<b>Conclusions</b>	<b>11</b>

---

## 1. Introduction

Round jets have been the focus of numerous experimental and numerical studies in the past. Considerable effort has been invested in this field in an effort to understand the evolution and the dynamics of the flow structure. Past experimental studies (e.g. [1, 2]) have established that the vorticity layer leaving the nozzle of the jet becomes unstable forming Kelvin–Helmholtz waves and then rolls up into vortex rings that are carried downstream where they become three dimensional and eventually break down. In addition to vortex rings, there is significant evidence (e.g. [3, 4, 2]) of streamwise structures, near both vortex cores and the regions between successive vortex cores in the shear layer called braids. Experiments by Lasheras *et al* [5] and numerical computations by Martin and Meiburg [6] illustrate the role of shearing forces acting perpendicular to the jet axis in the evolution of streamwise vorticity in the braid region. The experiments of Liepmann and Gharib [7] which examined planes normal to the axis of a water jet with Reynolds number ( $Re$ ) of 5500 indicate that three dimensionality first developed in the braid regions. Streamwise vortices were also observed in a high-Reynolds-number jet ( $Re = 78\,000$ ) by Paschereit *et al* [8]. Also, in a recent study by Citriniti and George [9], partial velocity field reconstruction of experimental data using POD indicated the presence of counter-rotating streamwise vortex pairs in the braid region between successive cores in a jet at  $Re = 80\,000$ .

Previous experimental studies have not had the capability of obtaining all three velocity components simultaneously in order to correlate and investigate the role of streamwise vorticity and the origin of three dimensionality in the near field of jets. Our primary objective is to study the evolution of three dimensionality with increasing axial distance and the role of streamwise vorticity in the evolution of three dimensionality in the flow. This paper reports on stereo PIV results obtained in the centreline plane of a round air jet. The resulting three-dimensional velocity vector fields were used to compute the in-plane gradients of the velocity components to investigate streamwise vorticity and its existence in various regions of the flow.

## 2. Experimental facility

A sketch of the jet facility that was used is shown in figure 1. The jet is driven by a six-blade fan, which in turn is powered by a standard DC power supply. The flow initially passes through a contraction and flow conditioning section consisting of screens and honeycomb. The flow then

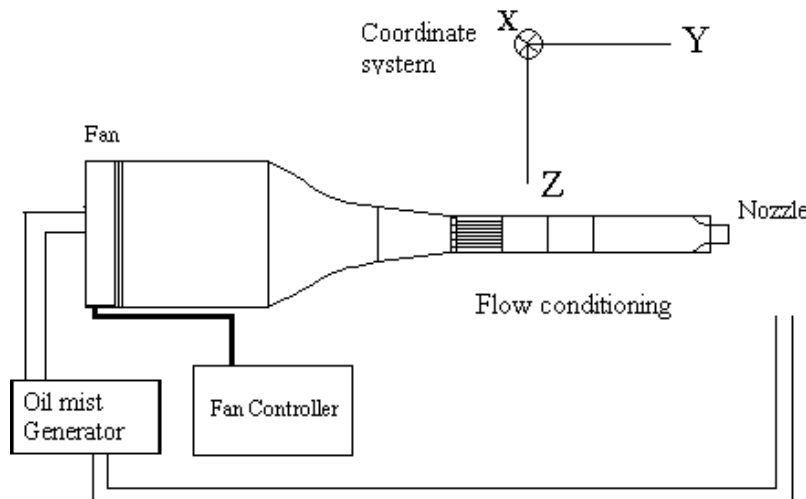


Figure 1. Jet facility.

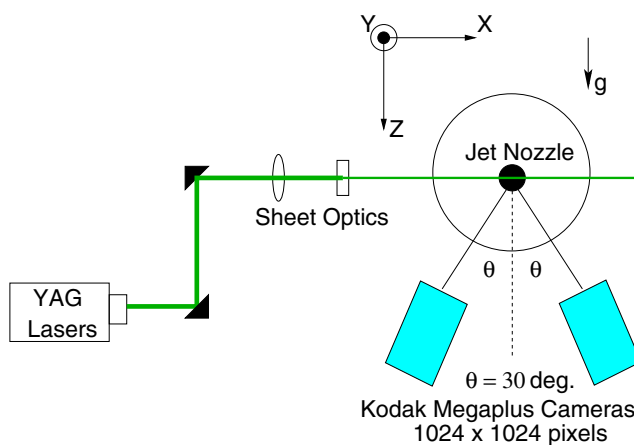


Figure 2. Experimental set-up.

passes through a second contraction and exits a nozzle with diameter ( $D$ ) of 30 mm. The second contraction follows a fifth-order polynomial curve. Both the jet and the ambient are seeded with olive oil droplets of size  $\sim 1 \mu\text{m}$ . The olive oil droplets are generated using Laskin nozzles and released just upstream of the fan as shown in figure 1. The ambient is seeded shortly before data acquisition. Hot-wire measurements near the jet exit reveal a top-hat profile and a centreline RMS velocity of less than 1% of the mean axial velocity ( $V_0$ ). Spectral measurements in the jet core show that the flow is not forced. Two pulsed Nd-YAG lasers were used to illuminate the centreline plane of the jet flow. A spherical bi-convex lens of focal length 1 m and a plano-concave cylindrical lens of focal length  $-25$  mm were used to convert each laser beam into a sheet. Two Kodak *Megaplug* cameras ( $1024 \times 1024$  pixels) captured the images. As shown in figure 2, the cameras were oriented at an angle  $\theta$  with respect to the perpendicular from the centre of the laser sheet. In this experiment, the angle  $\theta$  was fixed at  $30^\circ$  for both cameras. Note that the cameras are placed below the jet axis. The coordinate system in all the plots of the results is with respect to the camera and hence the results should be interpreted with the point of view that the flow is observed from beneath it.

### 3. Stereo PIV method

In this experiment we used the angular-displacement stereo PIV method in which the cameras are rotated inwards such that their axes intersect at the mid-point of the domain to be recorded as shown in figure 2. Since the object plane is not parallel to the lens plane, there is geometric distortion due to the perspective view. Therefore it becomes more difficult to obtain particle images that are well focused across the image plane. To overcome this problem, the Scheimpflug condition that requires the object, the lens, and the image planes to intersect at a common line, was enforced. This arrangement however introduces a strong perspective distortion and the magnification factor varies across the image plane. These issues can be overcome by calibrating the configuration.

#### 3.1. Calibration

The stereo PIV configuration was calibrated using a fixed grid (figure 3) that contains marker points with alternate points located in different planes. The two planes are separated by 1 mm in depth. This target was aligned with the laser sheet that illuminated the flow field. The cross mark at the centre of the image acts as a reference point for position. The image of the calibration target is captured by both cameras and analysed. The result of the analysis is a calibration file with a record of the image pixel location  $(x, y)$  and target marker location  $(X, Y, Z)$  for each marker in the image. Using these points, a set of mapping functions is generated for each camera:

$$x_{\text{left}} = f_1(X, Y, Z)$$

$$x_{\text{right}} = f_2(X, Y, Z)$$

$$y_{\text{left}} = f_3(X, Y, Z)$$

$$y_{\text{right}} = f_4(X, Y, Z)$$

where  $f$  is the generated mapping function. This set of mapping functions is used to compute the local displacements in seeded flow. After calibration, images are acquired, and an in-plane cross-correlation algorithm computes the relevant pixel displacements for each camera. The following set of transformation equations is used to obtain the fluid displacements:

$$dx_{\text{left}} = dX_{\text{fluid}} \left( \frac{dx_{\text{left}}}{dX} \right) + dY_{\text{fluid}} \left( \frac{dx_{\text{left}}}{dY} \right) + dZ_{\text{fluid}} \left( \frac{dx_{\text{left}}}{dZ} \right)$$

$$dy_{\text{left}} = dX_{\text{fluid}} \left( \frac{dy_{\text{left}}}{dX} \right) + dY_{\text{fluid}} \left( \frac{dy_{\text{left}}}{dY} \right) + dZ_{\text{fluid}} \left( \frac{dy_{\text{left}}}{dZ} \right)$$

$$dx_{\text{right}} = dX_{\text{fluid}} \left( \frac{dx_{\text{right}}}{dX} \right) + dY_{\text{fluid}} \left( \frac{dx_{\text{right}}}{dY} \right) + dZ_{\text{fluid}} \left( \frac{dx_{\text{right}}}{dZ} \right)$$

$$dy_{\text{right}} = dX_{\text{fluid}} \left( \frac{dy_{\text{right}}}{dX} \right) + dY_{\text{fluid}} \left( \frac{dy_{\text{right}}}{dY} \right) + dZ_{\text{fluid}} \left( \frac{dy_{\text{right}}}{dZ} \right)$$

where  $(dx_{\text{left}}, dy_{\text{left}})$  and  $(dx_{\text{right}}, dy_{\text{right}})$  are the pixel displacements from cross-correlation, and  $(dX, dY, dZ)$  are the unknown fluid displacements. The coefficients within the parentheses, displacement gradients with respect to the fluid space, are obtained from the mapping functions generated by calibration. This system of four equations with three variables is solved using a least-squares error method. To obtain a three-dimensional vector field with more than 95%

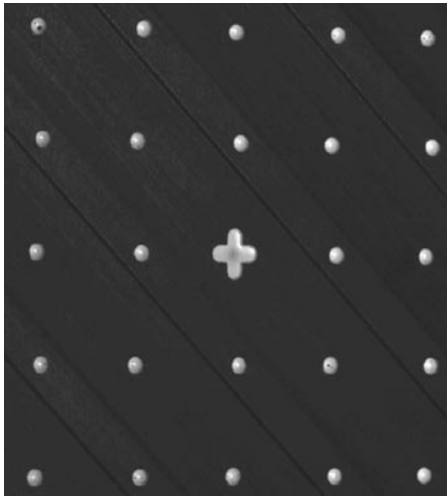


**Figure 3.** A portion of the calibration target. The marker points are 10 mm apart.

valid vectors, it is imperative that the calibration is of very high quality. The two cameras must be focused at the same plane and location, and the system should not experience any kind of physical disturbance between the calibration process and data acquisition. The calibration coefficients and the mapping functions were computed using TSI *Pivcalib* software. A TSI Laser pulse synchronizer box was used to control the strobing and timing of the cameras and the lasers. This box was controlled by TSI *Insight (3.2)* software. The same software also computed pixel and fluid displacements.

### 3.2. Sources of uncertainty

The major sources of uncertainty in computing the velocity vectors were bias due to peak fitting in correlation calculations and bias generated in curve fitting. Uncertainty in the cross-correlation peak location algorithm depends on pixel displacement, interrogation spot size, presence of displacement gradients within the spot, etc. In this experiment the interrogation spots were  $32 \times 32$  pixels with 50% overlap, and the magnification was about  $50 \mu\text{m}/\text{pixel}$ . In general, displacement uncertainties were of the order of 0.1 pixels for the Gaussian peak-finding algorithm. The resulting uncertainty at all points was less than 1% of the jet exit velocity. Bias error arises due to the curve fit resulting from the system of four equations in three variables. For a given image set, the calibrated system solution is substituted back into the equations to determine the accuracy of the fit. The difference between the planar pixel displacements calculated by cross-correlation and the pixel displacement obtained by substituting the calibration solution are recorded as ‘residual pixels’ (figure 4). The value of the residual is a measure of the credibility of the three-dimensional vector field. The residual values were usually highest in regions with strong velocity gradients. This is because the left and right cameras can record different pixel displacements for a single interrogation spot based on their different perspectives. Such differences cause errors in the curve fit when the reconstruction software attempts to match the left and right camera vectors. Plots of residual pixels reveal values less than 0.1 pixels ( $< 0.01V_0$ ) in the core of the jet and less than 0.6 pixels ( $< 0.06V_0$ ) in the shear layer for  $y/D > 1$ . The residual pixels range from 0.8 to 1.5 pixels ( $0.08\text{--}0.15V_0$ ) in a very limited and narrow region just downstream of the jet exit where the velocity and seeding concentration gradients are very high. Analysis over many image sets indicates that disparities in streamwise pixel displacement

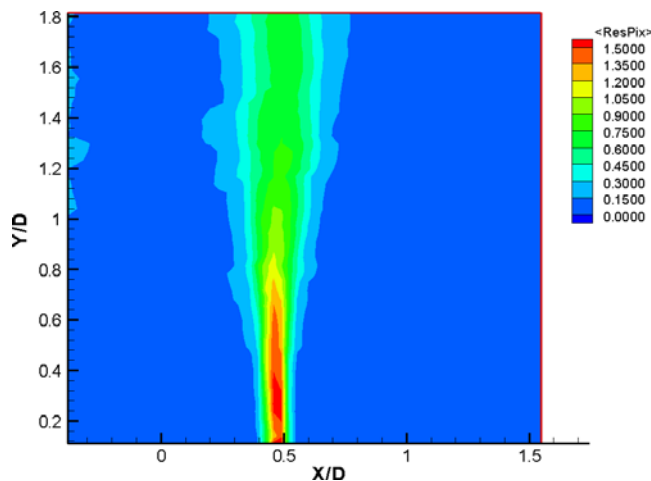


Figure 4. Average residual pixels.

in the two cameras contribute more significantly to the residual pixels than spanwise/radial displacements due to the fact that the streamwise displacements have relatively high magnitudes.

#### 4. Results and discussion

Three-dimensional vector fields were computed for more than 300 realizations at various downstream locations. Mean and RMS statistics were computed from ensemble averages of the velocity fields. All computed quantities are made dimensionless using the jet centreline exit velocity  $V_0 = 9.45 \text{ m s}^{-1}$  and jet exit nozzle diameter  $D = 30 \text{ mm}$ . The corresponding jet Reynolds number was 19 000.

The coordinate system used to describe the results is right handed with the axial direction (streamwise) of the jet being represented by the  $Y$ -axis (see figures 1 and 2). Since the images were taken in the centreline plane of the jet, the  $X$ - and  $Z$ -axes are the radial and azimuthal directions respectively. The origin is located at the centreline of the jet exit. The quantities  $V$ ,  $U$ , and  $W$  represent the axial, radial, and azimuthal velocity components respectively. The results show only the right side (if seen from below) of the jet shear layer. All gradients of velocities were computed using a second-order finite-difference scheme within the domain and a first-order scheme on the boundaries. This translates to using only the immediate neighbours of a grid point in the computation. The gradients were computed over a resolution of  $0.064D \times 0.064D$ .

##### 4.1. Mean and RMS statistics

The axial mean velocity contours in figure 5(a) clearly indicate that the core of the jet has a uniform axial velocity distribution and that the shear layer grows with downstream distance. The plot of RMS axial velocity (figure 5(b)) reveals values of nearly  $0.2V_0$  in the shear layer and less than  $0.02V_0$  in the jet core. Figure 6(a) shows the mean radial velocity component. It is clear from the figure that the radial mean is low in the jet core while it deviates from zero in both directions in the shear layer. The radial mean is positive on the inner side and negative on the outer side of the shear layer as expected, and the RMS velocity follows the axial velocity behaviour. The RMS of the radial velocity (figure 6(b)) is less than  $0.02V_0$  in the core of the jet and more than  $0.1V_0$  in the shear layer. It increases downstream of  $y/D = 0.4$  reaching a maximum value of about  $0.18V_0$  at  $y/D = 1.7$ . This is the region where the Kelvin–Helmholtz

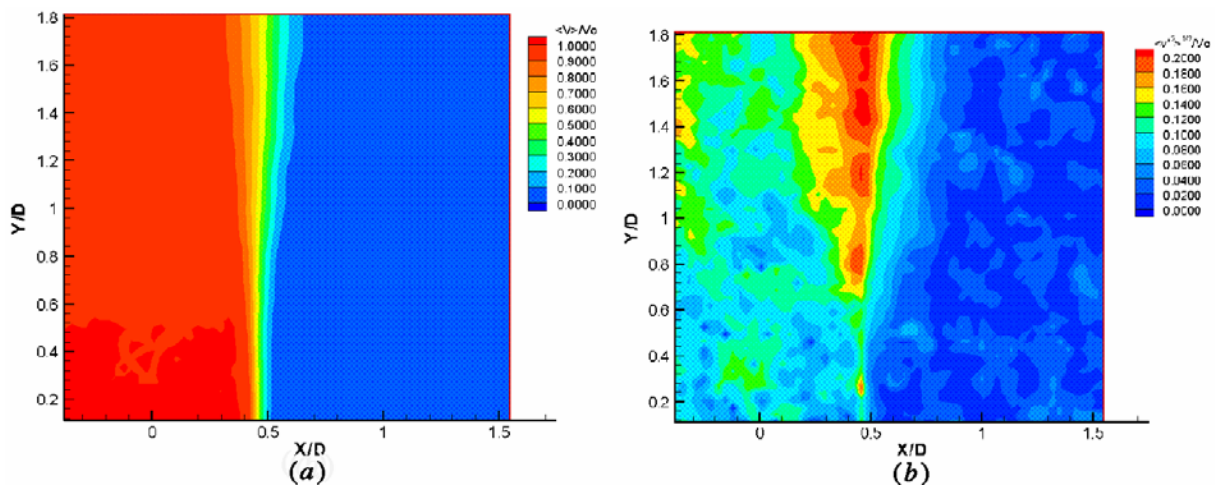


**Figure 5.** Axial velocity statistics in the near field of the jet. (a) Mean  $\langle V \rangle$ , (b) RMS.

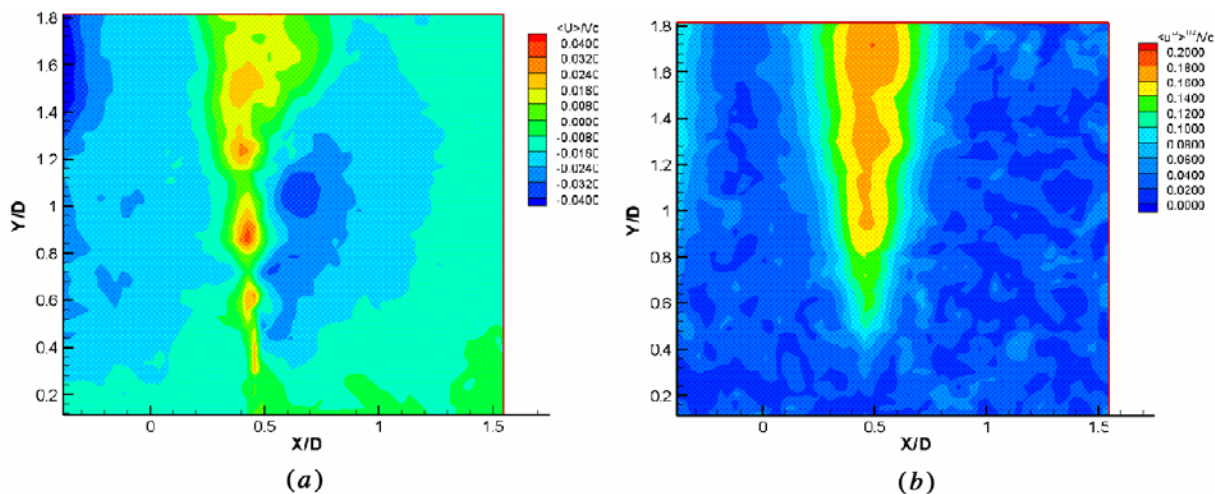


**Figure 6.** Radial velocity statistics in the near field of the jet. (a) Mean  $\langle U \rangle$ , (b) RMS.

waves become unstable, resulting in vortex sheet roll up and formation of vortex rings. The mean and RMS of the azimuthal component were also computed. The mean field reveals that the azimuthal velocity field is close to zero across the entire field of view with the range being  $-0.01$  to  $0.01V_0$ . The RMS of the azimuthal velocity indicates smaller values than those found for the radial and axial components. The RMS values in the shear layer are of the order of  $0.1V_0$  downstream of  $y/D = 0.4$  and the maximum value in the field was  $0.13V_0$ . A general trend of increasing RMS values with downstream distance is also noticed in all three components.

## 4.2. Vortex identification

To study the interesting features of the flow and any coexistence of three dimensionality and azimuthally coherent vortex rings, we need a tool to identify coherent structures. Vortex cores can be identified visually in an image (see figure 7(a)), but to identify them in a velocity field is more

challenging. Different quantities have been used in the past to identify the various important features of the flow. In this section, we illustrate the use and the effectiveness of four such quantities.

*Vorticity* is one such quantity that will show the presence of the swirling motion. The out-of-plane component of vorticity ( $\omega_z$ ) was used to detect the interesting regions in the flow. *Swirl strength* ( $\lambda_{ci}$ ) [11] is a derived quantity that isolates the coherent swirling structures. It is the imaginary part of the eigenvalue of the velocity gradient tensor. This concept of using the complex eigenvalues to detect vortices was proposed by Chong *et al* [13].  $D^*$  is the discriminant of the characteristic equation of the two-dimensional velocity gradient tensor [12]. This quantity will illustrate regions of swirl and strain. The parameter  $\lambda_{ci}$  is a subset of  $D^*$ . The eigenvalue of the tensor will be imaginary only in the regions where  $D^*$  is negative. And finally,  $Q$  which is defined as the second invariant of the velocity gradient tensor (see [14] and [15]) was computed. For incompressible flows,

$$Q = -\frac{1}{2}u_{i,j}u_{j,i} = \frac{1}{2}(\text{tr}[\Omega\Omega^t] - \text{tr}[SS^t]) \quad \text{and} \quad u_{i,j} = \frac{\partial u_i}{\partial x_j}$$

where  $S$  and  $\Omega$  are the symmetric and antisymmetric part of the velocity gradient tensor. For *two-dimensional* incompressible flows it can be shown that  $D^* = -4Q$ .

It is very important to note that all quantities were computed with just the in-plane velocity gradients, and hence we considered only the components of the two-dimensional velocity gradient tensor.

A raw image of an instantaneous flow field is shown in figure 7(a) and the out-of-plane vorticity ( $\omega_z$ ) behaviour for the same image is shown in figure 7(b). Vorticity does indeed detect regions of swirl but was unable to differentiate between a vortex sheet (as seen just downstream of the jet exit) and a vortex core. The failure of vorticity to isolate the coherent structures led to the use of swirl strength (figure 7(c)) which performs well in identifying the regions of swirl, in this case the vortex cores. The figure shows contours of  $\lambda_{ci}^2$ . The negative values of  $\lambda_{ci}^2$  result in imaginary eigenvalues and consequently indicate the presence of swirling motion. However, this quantity does not give any insight into the straining zones. The quantity  $Q$  was computed for the image set corresponding to figure 7(a), and the result is given in figure 7(d). Large positive values of  $Q$  suggest the presence of a vortex core and negative values indicate a straining region. The discriminant ( $D^*$ ) has a behaviour similar to that of  $Q$  (see figure 7(e)), with the difference being that positive values of  $D^*$  indicate straining zones and negative values describe the regions of swirl. One other difference between the two quantities is that the identified regions in  $D^*$  have larger areas than in  $Q$  due to the out-of-plane motion in the flow, as the jet flow is not completely two dimensional. It can be noted that both of these quantities perform well in identifying the interesting features of the flow. In this paper, we will use  $Q$  to illustrate the various regions in the flow field.

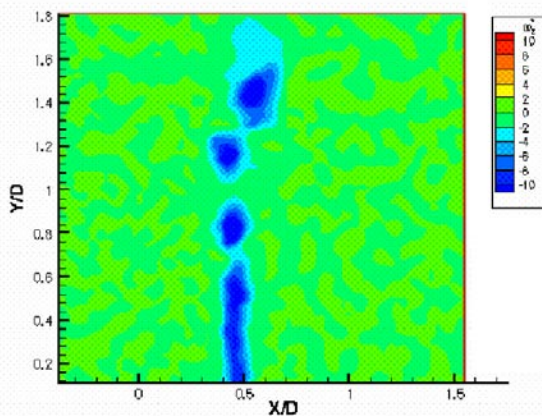
### 4.3. Three dimensionality

The raw image and the quantity  $Q$  of an instantaneous field are shown in figures 8(a) and (b). The azimuthal velocity  $W$  (figure 8(c)) and a component of the streamwise vorticity ( $\partial W/\partial X$ ) (figure 8(d)) were computed for the same image set. The plot of  $W$  demonstrates the degree of instantaneous three dimensionality in the near field of the jet. The magnitudes of the azimuthal velocity are of the order of  $\pm 0.2V_0$  and  $\pm 0.3V_0$  near the vortex cores at  $y/D = 0.9$  and  $1.6$  respectively. The magnitudes of the azimuthal velocity are large ( $0.15-0.2V_0$ ) in the straining braid regions between the two vortex cores. Such large magnitudes were not found in previous studies until further downstream. For example, in a jet with  $Re = 52\,000$  [10], a stereo PIV plot normal to the jet axis showed relative magnitudes of the azimuthal velocity at  $y/D = 2.0$  similar to those observed in this study at  $y/D = 0.9$ .

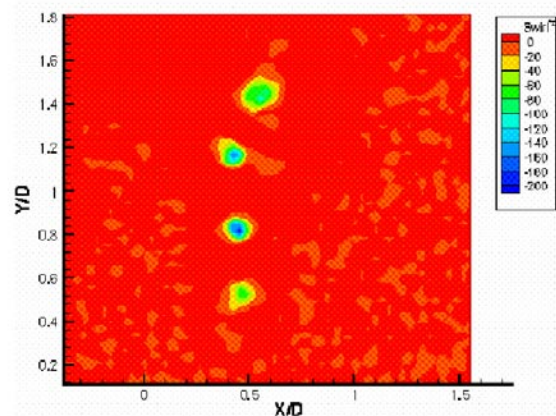
## Investigation of three dimensionality in the near field of a round jet using stereo PIV



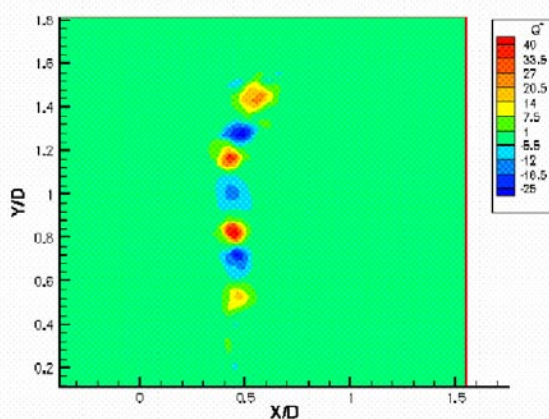
(a)



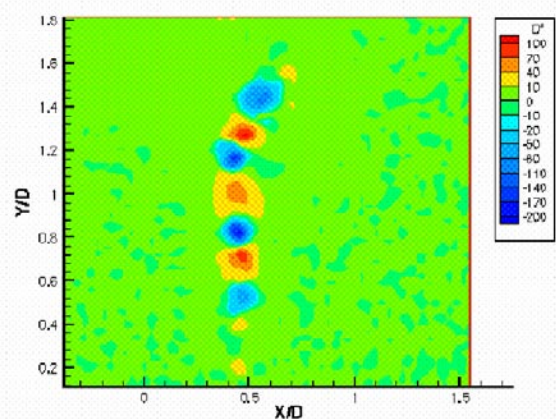
(b)



(c)



(d)



(e)

**Figure 7.** Instantaneous quantities in the near field ( $y/D = 0-2.8$ ). (a) Raw image, (b) vorticity, (c) swirl, (d)  $Q$  and (e)  $D^*$ .

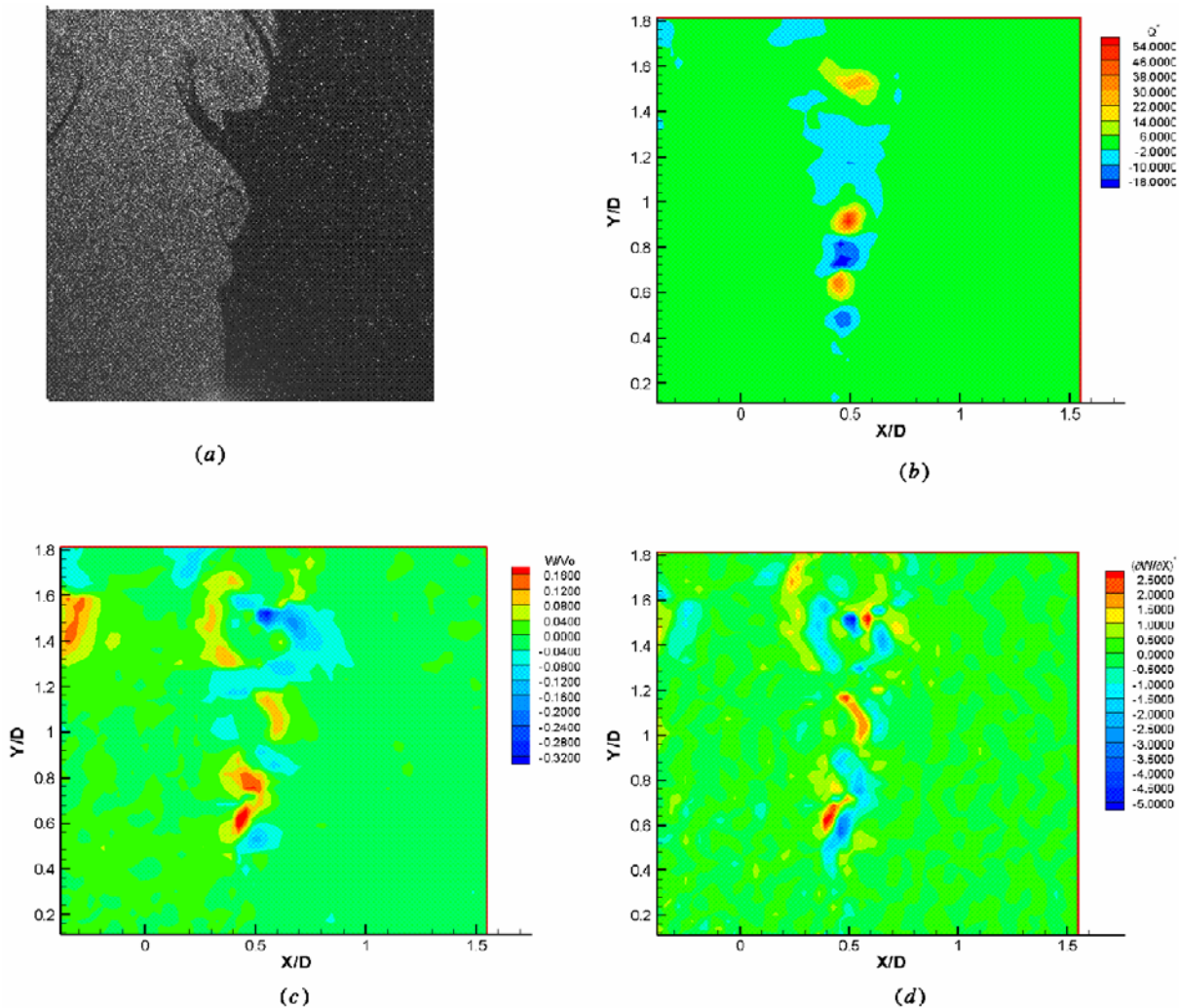


**Figure 8.** Instantaneous quantities in the near field ( $y/D = 0-2.8$ ). (a) Raw image, (b)  $Q$ , (c)  $W$  and (d)  $\partial W/\partial X$ .

The significant positive and negative  $W$  near the vortex core indicate either bending of the core or azimuthal swirl within the core. The braid stretching downstream ( $y/D = 1.0-1.4$ ) straddles strong positive and negative strips of  $W$  (see figures 8(b)–(d)). The plot of  $\partial W/\partial X$  displays a very clear pattern of sign changes surrounding the braid and the vortex cores. This indicates the presence of vortex tubes inclined with respect to the streamwise-radial plane similar to the mushroom pairs observed by Liepmann and Gharib [7] in their flow visualization. Examination of many images indicates that the three dimensionality and the structural patterns shown here occur very frequently. Analysis of additional plots of  $Q$  and  $W$  suggests that the first signs of significant azimuthal velocity appear in the straining region just upstream of the first vortex core. In this experiment, this region occurs at about  $y/D \sim 0.5$ .

Investigation of velocity fields further downstream illustrates the growth of three dimensionality. The original vortex cores pair into rings separated by greater axial distances and stronger, longer straining regions (see figures 9(a) and (b)). Note that the straining zone in figure 9(b) is closely connected to the downstream vortex core but not the upstream one. The plot of azimuthal velocity (figure 9(c)) shows a pair of zones with positive and negative values

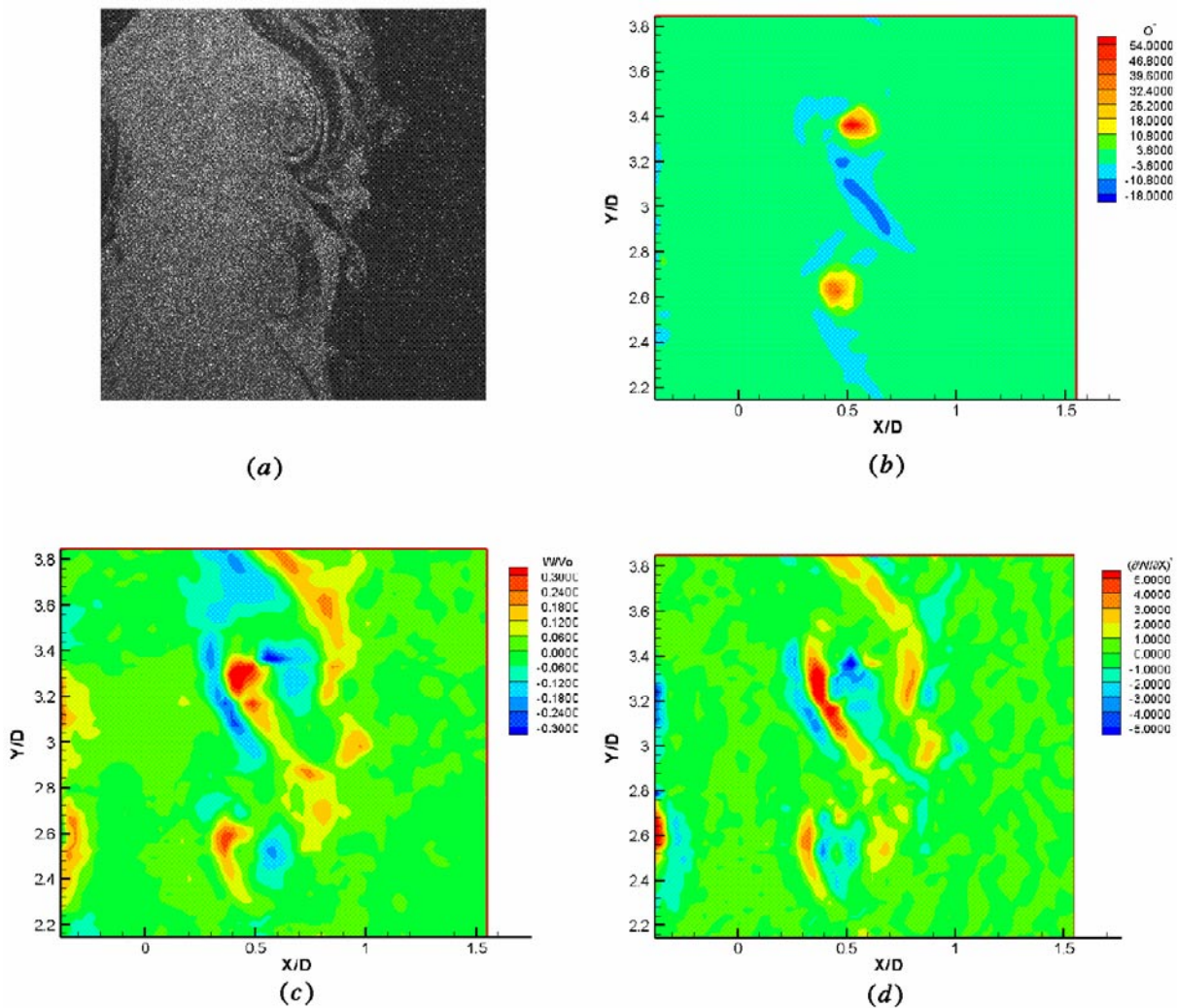


**Figure 9.** Instantaneous quantities in the near field ( $y/D = 3-5.8$ ). (a) Raw image, (b)  $Q$ , (c)  $W$  and (d)  $\partial W/\partial X$ .

just upstream of each core centre. Typically, these zones have larger size and velocity magnitude than corresponding zones closer to the nozzle exit. The streamwise vorticity component  $\partial W/\partial X$  (figure 9(d)) also shows longer strips of greater magnitude than were observed upstream. As before, these strips are oriented at an angle that suggests the existence of streamwise vortex tubes in the braid regions. It is observed from the plots of the azimuthal velocity component ( $W$ ) that these streamwise vortex tubes advect high-momentum fluid from the potential core to the slower shear layer and vice versa depending on the direction of vorticity as noted by various other researchers (see [6, 7] and [9]).

## 5. Conclusions

Stereo particle image velocimetry was employed successfully in measuring all three instantaneous velocity components in the centreline plane of a round air jet of Reynolds number 19 000. The measurements were taken in the near field of the jet. The mean and RMS statistics were

computed, and the results agree with previous work. The RMS values of the axial and radial velocity components are high in the shear layer ( $\sim 0.15V_0$ ) and low in the core of the jet ( $\sim 0.01V_0$ ). The RMS of the azimuthal velocity increases with the downstream distance and reaches a maximum value of  $0.13V_0$  in the shear layer.

A vortex identification scheme that involved the use of  $Q$  as a flow identifier was employed to correlate the presence of vortex core or straining braid regions with the azimuthal component of the velocity to understand the evolution of three dimensionality. The performance and effectiveness of several other parameters such as swirl strength, vorticity, and discriminant in detecting the interesting regions in the flow were also assessed.

Investigation of the instantaneous fields reveals that the flow is three dimensional in the near field beginning at  $y/D \sim 0.5$  in the straining region immediately upstream of the first vortex core formed due to Kelvin–Helmholtz instability. This result is significantly earlier than those reported in previous studies. The small-scale vortex cores in the near field evolve and pair up with the vortices upstream to form larger-scale structures downstream as observed in the images and the velocity fields. Analysis of the azimuthal velocity and its derivatives clearly indicates the presence of inclined vortex tubes in the braid region connecting successive vortex cores.

## Acknowledgments

The authors wish to thank Arnaud Loyer, an exchange student (from department of fluid and transfer dynamics, Ecole Centrale de Nantes, France) for being instrumental in setting up the experiment. The support of the National Science Foundation is gratefully acknowledged, through grant no ACI-9982274.

## References

- [1] Crow S C and Champagne F H 1971 Orderly structures in jet turbulence *J. Fluid Mech.* **48** 547
- [2] Yule A J 1978 Large scale structures in the mixing layer of a round jet *J. Fluid Mech.* **89** 413
- [3] Becker H A and Masaro T A 1968 Vortex evolution in a round jet *J. Fluid Mech.* **31** 435
- [4] Agui J C and Hesselink L 1988 Flow visualization and numerical analysis of a coflowing jet: a three-dimensional approach *J. Fluid Mech.* **191** 19
- [5] Lasheras J C, Cho J S and Maxworthy T 1986 On the origin and evolution of streamwise vortical structures in a plane free shear-layer *J. Fluid Mech.* **172** 231
- [6] Martin J E and Meiburg E 1991 Numerical investigation of three-dimensionally evolving jet subject to axisymmetric and azimuthal perturbations *J. Fluid Mech.* **230** 271
- [7] Liepmann D and Gharib M 1992 The role of streamwise vorticity in the near-field entrainment of round jets *J. Fluid Mech.* **245** 643
- [8] Paschereit C O, Oster D, Long T A, Fiedler H E and Wygnanski I 1992 Flow visualization of interactions among large coherent structures in an axisymmetric jet *Exp. Fluids* **12** 189
- [9] Citriniti J H and George W K 2000 Reconstruction of global velocity field in the axisymmetric mixing layer utilizing the proper orthogonal decomposition *J. Fluid Mech.* **418** 137
- [10] Gaydon M, Raffel M, Willert C, Rosengarten M and Kompenhans J 1997 Hybrid stereoscopic particle image velocimetry *Exp. Fluids* **23** 331
- [11] Zhou J, Adrian R J, Balachandar S and Kendall T M 1999 Mechanisms for generating coherent packets of hairpin vortices in channel flow *J. Fluid Mech.* **387** 353
- [12] Blackburn H M, Mansour N M and Cantwell B J 1996 Topology of fine scale motions in turbulent channel flows *J. Fluid Mech.* **310** 269
- [13] Chong M S, Perry A E and Cantwell B J 1990 A general classification of three-dimensional flow fields *Phys. Fluids A* **2** 765
- [14] Jeong J and Hussain F 1995 On identification of a vortex *J. Fluid Mech.* **285** 65
- [15] Dubief Y and Delcayre F 2000 On coherent structure identification in turbulence *J. Turbulence* **1** 011